Journal of Applied Polymer Science

Influences of Compatibilizers on Rheology and Mechanical Properties of Propylene Random Copolymer/Styrene-ethylene-butylene-styrene Block Copolymer/Organic-Montmorillonite Nanocomposites

Binbin Liu, Yonggang Shangguan, Yihu Song, Qiang Zheng
Key Laboratory of Macromolecular Synthesis and Functionalization of Ministry of Education, Department of Polymer Science and Engineering, Zhejiang University, Hangzhou 310027, People's Republic of China
Correspondence to: Q. Zheng (E-mail: zhengqiang@zju.edu.cn)

ABSTRACT: Propylene random copolymer (PPR)/styrene-ethylene-butylene-styrene block copolymer (SEBS)/compatibilizer/organic-montmorillonite (OMMT) quaternary nanocomposites and PPR/compatibilizer/OMMT ternary nanocomposites were prepared via two-stage melt blending and influences of compatibilizers, maleic anhydride (MA) grafted styrene-ethylene-butylene-styrene copolymer (SEBS-*g*-MA), poly(octene-*co*-ethylene) (POE-*g*-MA), or propylene block copolymers (PPB-*g*-MA), on rheology and mechanical properties of the nanocomposites were investigated. The results of X-ray diffraction measurement and transmission electron microscopy observation showed that OMMT layers were mainly intercalated in the nanocomposites except for the mainly exfoliated structure in the quaternary nanocomposites using POE-*g*-MA as compatibilizer. The nanocomposites exhibited pseudo-solid like viscoelasticity in low frequencies and shear-thinning in high shear rates. As far as OMMT dispersion was concerned, POE-*g*-MA was superior to SEBS-*g*-MA and PPB-*g*-MA, which gives rise to the highest viscosities in both the ternary and quaternary nanocomposites. The quaternary nanocomposites containing POE-*g*-MA were endowed with balanced toughness and rigidity. It was suggested that a suitable combination of compatibilizer and SEBS was an essentially important factor for adjusting the OMMT dispersion and distribution, the rheological and mechanical performances of the nanocomposites. © 2012 Wiley Periodicals, Inc. J. Appl. Polym. Sci. 129: 973–982, 2013

KEYWORDS: nanostructured polymers; polyolefins; thermoplastics; viscosity and viscoelasticity; structure-property relations

Received 26 March 2012; accepted 23 September 2012; published online 22 November 2012
DOI: 10.1002/app.38637

INTRODUCTION

Over the past two decades, organic–inorganic nanocomposites have attracted many academic and industrial interests due to their excellent properties synergistically derived from their original components.[1–4] As a kind of layered silicates, montmorillonite (MMT) has been commonly used to prepare polymer nanocomposites (PNCs) to improve mechanical, thermal, barrier as well as other properties of polymer materials.[5]

It has been found that mechanical properties of PNCs are closely related to the dispersion of MMT layers in the matrix.[6–9] Many researchers have paid their focuses on the dispersion of organically modified MMT (OMMT) and morphology of PNCs. In general, the exfoliated dispersion is superior to the intercalated one.[10] However, PNCs filled with OMMT seldom reaches an optimum balance between impact strength and stiffness.[11] A good OMMT dispersion even at contents less than 5 wt % would decrease impact resistance of PCNs especially at low temperatures, which could be ascribed to the relatively high glass transition temperature (T_g) of PNCs and poor interface adhesion between the filler and the matrix.[5,12] Some elastomers such as ethylene-propylene-diene monomer rubber (EPDM), poly(octene-*co*-ethylene) (POE) and styrene-ethylene-butylene-styrene (SEBS) copolymer etc. are thus introduced to toughen PNCs.[6,13–15]

SEBS has been used to toughen polymers while sometimes lowers rigidity and strength.[16,17] Maleated SEBS (SEBS-*g*-MA) is beneficial to enhance work of fracture of isotactic polypropylene (iPP)/OMMT PNCs.[17,18] Hence, ternary PNCs comprising polymer, SEBS and filler are designed for overcoming the shortages of reinforcement using inorganic filler and toughening using thermoplastic elastomer solely. SEBS and SEBS-*g*-MA have been used to modify viscoelasticity of polyamide 6/OMMT PNCs.[19] It is noted that iPP-*g*-MA is frequently used to control the selective locations of OMMT in one, or another of the polymers or at the iPP-SEBS interface,[20,21] leading to a slight increase in notched impact toughness, stiffness, and strength as compared with iPP/SEBS blend.[22]

Table I. Characteristics of the Raw Materials Used

Sample code	Trademark	MA content (wt %)	MFI (g/10 min)	M_w	M_w/M_n	η^* at 170°C (kPa s)
PPR	PPC0723	-	7	328,892	5.01	2.4
SEBS	MD6945M[a]	-	2.0–4.5	236,534	1.37	12.3
SEBS-*g*-MA	FG1901X[a]	1.8	14–28[b]	56,723	1.43	10.4
POE-*g*-MA	POE-G-1	0.9	0.5–2.5[c]	201,308	5.06	2.4
PPB-*g*-MA	CMPP3015	0.9	120[d]	136,688	4.91	0.37

[a]Styrene/rubber ratio = 30/70, [b]230°C/5.0 kg, [c]190°C/2.16 kg, [d]230°C/2.16 kg.

Since, compatibilizer is an important factor in determining the dispersion of OMMT layers, it is necessary to understand the effects of various compatibilizers with different molecular structures on PNCs. Previous studies have attempted to improve mechanical properties of PNCs with ealstomeric tougher or compatibilizer,[17–19,22,23] whereas there is few systematical research on the combined effect of elastomeric tougher and compatibilizer on OMMT dispersion and distribution in PNCs. The present article aims at the preparation, structure, and properties of PNCs based on ethylene-propylene random copolymer (PPR) containing less than 5% ethylene monomer. SEBS is introduced for toughening PNCs and three compatibilizers, SEBS-*g*-MA, POE-*g*-MA, and propylene block copolymer (PPB)-*g*-MA, are used for improving OMMT dispersion through traditional mechanical compounding technique. This article will provide a more detailed understanding of the effect of compatibilizer and its combination with SEBS on the OMMT dispersion and distribution in PNCs. Furthermore, such a study would provide a complementary insight into relationships between rheological behaviors of PNCs with their microstructures. Finally, the mechanical properties of PNCs with or without SEBS are investigated for outlining PNCs design to achieve a preferred balance of material performances.

EXPERIMENTAL

Materials

PPR (PPC0723, ethylene content 3.0 wt %, melt flow index MFI = 7 g/10 min at 230°C/2.16 kg, weight averaged molecular weight M_w = 328,892 and molecular distribution index M_w/M_n = 5.01) was supplied by Dushanzi Petrochem, China. SEBS (MD6945M, M_w = 236,534 and M_w/M_n = 1.37) was a product from Kraton Performance Polymers, USA. OMMT (Nanomer I31PS) with a cationic exchange capacity 145 meq/100 g was a product from Nanocor, USA, which was modified using aminopropyltriethoxysilane and octadecylamine. The compatibilizers, maleic anhydride (MA) grafted SEBS triblock copolymer, poly(octene-*co*-ethylene) and block copolymer of propylene, abridged as SEBS-*g*-MA, POE-*g*-MA, and PPB-*g*-MA, were obtained from Kraton Performance Polymers, USA, Nanjing Deba Chem., China and Chenguang Research Institute of Chem. Industry, China, respectively. Some main parameters of the raw materials are listed in Table I.

Preparation of PNCs

A two-stage extrusion method was used to prepare PNCs on a corotating twin-screw extruder (Haake Rheomex PTW16/40 OS, Thermo Fish Sci., Germany) with a diameter of 16 mm and a length-to-diameter ratio of 40. The temperature profile (from feeding to die) was 160, 165, 170, 170, 170, 175, 170, 170, 170, and 170°C, and the screw rotation speed was 250 rpm. Such temperature profile for preparing PNCs was designed mainly according to the onset thermal decomposition temperature of OMMT and the end melting temperature of PPR for achieving the maximum screw shear stress. A PPR masterbatch containing 15 wt % OMMT was prepared in the first extrusion and the PNCs with 2 wt % OMMT were prepared in the second extrusion. Table II shows compositions of the ternary (PPR/compatibilizer/OMMT, termed as PPR series) and the quaternary (PPR/SEBS/compatibilizer/OMMT, termed as PPRS series) PNCs with 3 wt % compatibilizer and 2 wt % OMMT. Samples were prepared by compression molding at 180°C under 15 MPa.

Characterization

XRD. X-ray diffraction (XRD) measurements were conducted on a Rigaku D/Max 2550PC apparatus (Rigaku Mechatronics, Japan) equipped with an incident X-ray of Cu Kα. The operating condition of the X-ray source was set at a voltage of 40 kV and a current of 100 mA. A step of 0.02° was adopted to scan in range of 2θ from 0.5° to 40°.

TEM. The samples were cut into ultrathin films using an ultramicrotome (Reichert-Jung F4-CD, Rigaku Mechatronics, Japan) and were observed on a transmission electron microscopy (TEM, JEM-1200EX, Japan) with an accelerating voltage of 120 kV.

SEM. The samples fractured in Izod impact tests at room temperature were observed on a scanning electron microscopy (SEM, Hitachi S4800, Japan) at 3.0 kV voltage at magnifications varying from 400× to 5000×.

Rheology. Rheological experiments at 180°C were conducted on an advanced Rheometer Expansion System (ARES-G2, TA Instruments-Waters LLC, USA) with a parallel-plate fixture (25 mm diameter). Disk samples were compression molded into 1.2 mm in thickness and 25 mm in diameter. The gap between the two parallel plates was maintained at 0.9 mm by automatic adjustment. Dynamic strain (γ) sweep experiments were carried out at 10 rad/s to distinguish the linearity region, and dynamic frequency (ω) sweep from 0.01 to 100 rad/s were performed in the linearity region. Steady flow experiments were performed in a shear rate ($\dot{\gamma}$) range from 0.001/s to 100/s.

Mechanical Properties. Tensile properties were tested using a universal tester (SANS CMT4204, MTS System, China) according to GB/T 1040 (equivalent to ISO 527: 1995) at a stretching speed of 500 mm/min at room temperature. The bars were

Table II. Interlayer Spacing (d_{001}), Critical Shear Rate for Thinning ($\dot{\gamma}_c$) and Zero-Shear Viscosity (η_0) of the PNCs with Different Compositions

Sample code	Compatibilizer	Composition (PPR/SEBS/compatibilizer/ OMMT by weight)	2θ (°)	d_{001} (nm)	$\dot{\gamma}_c$ (1/s)	η_0 (kPa s)
I31PS	/	/	3.99	2.21	/	/
PPR	/	100/0/0/0	/	/	0.040	5.7
PPR1	SEBS-*g*-MA	95/0/3/2	3.40	2.60	0.040	6.2
PPR2	POE-*g*-MA	95/0/3/2	3.12	2.83	0.063	6.2
PPR3	PPB-*g*-MA	95/0/3/2	3.46	2.55	0.025	5.8
PPRS	/	85/15/0/0	/	/	0.016	8.6
PPRS1	SEBS-*g*-MA	81/14/3/2	3.42	2.58	0.010	11.2
PPRS2	POE-*g*-MA	81/14/3/2	/	/	0.010	11.0
PPRS3	PPB-*g*-MA	81/14/3/2	3.42	2.58	0.016	10.0

prepared by cutting samples from the middle of the compression molded sheets. An average of five duplicates for each sample was adopted.

Izod impact tests were carried out using an Izod impact tester (SANS ZBC 1400-2, MTS System, China) at room temperature and −23°C, respectively, according to GB/T 1843 (equivalent to ASTM D 256-05). The specimens were processed into notches using an automatic notched impact sample system prototype. An average of ten duplicates for each sample was adopted.

RESULTS AND DISCUSSIONS

Effect of Compatibilizers on Microstructure of PNCs

Figure 1 shows XRD patterns of the ternary and the quaternary PNCs. The diffraction peak appeared at 2θ from 0.5° to 6.0° is involved in the OMMT dispersion. Interlayer spacing (d_{001}) calculated from the peak position and the wavelength of incidental radiation ($\lambda = 1.54$ Å) according to Bragg's Law is listed in Table II. d_{001} of the PNCs are about 0.3–0.6 nm higher than that of OMMT except for PPRS2 compatibilized by POE-*g*-MA, which exhibits an exfoliated morphology as expected from the disappearance of the diffraction peak. d_{001} of PPR1, PPR3, PPRS1, and PPRS3 is almost equal and is lower than that of PPR2 and PPRS2, suggesting that POE-*g*-MA could promote dispersion of more intercalated or exfoliated OMMT than SEBS-*g*-MA and PPB-*g*-MA in both the ternary and the quaternary PNCs. Lai et al.[24] found that POE-*g*-MA can improve PP intercalation into OMMT more effectively than PP-*g*-MA. The mainly exfoliated OMMT dispersion is obtained only when POE-*g*-MA is used as compatibilizer in the quaternary PNCs, indicating that POE-*g*-MA in combination with SEBS can effectively exfoliate OMMT. Though strong hydrogen bonding between hydroxyl groups of silicates and MA functional group of the compatibilizer may be essential for promoting the OMMT dispersion,[13,25] the effect is highly dependent on chemical structure of the compatibilizer. Using the same compatibilizer POE-*g*-MA, the ternary PPR2 shows the highest intercalation degree and the quaternary PPRS2 shows the main exfoliation dispersion of OMMT, indicating that POE-*g*-MA is more effective in the quaternary PNCs than in the ternary PNCs on promoting OMMT dispersion and enhancing intercalation of the polymer chains into interlayers of OMMT. The results differ from Sun et al.,[13,15] who found that the coexistence of POE as an elastomeric modifier and PPB-*g*-MA as a compatibilizer did not significantly affect the OMMT intercalation and exfoliation in iPP/POE/OMMT composites. The intercalated morphology of the ternary PNCs with PPB-*g*-MA compatibilizer agrees with Su and Huang[22] who observed the same OMMT distribution in iPP-*g*-MA compatibilized iPP/OMMT and iPP/SEBS/OMMT PNCs.

Figure 2 shows TEM images of the PNCs. The samples except for PPR3 were stained by RuO_4 solution for 12 h so that the SEBS-rich domains are gray-colored in the TEM images while the white background represents PPR. OMMT aggregates in dark color are easily distinguished especially in the zoomed-out images in the insets. OMMT is rather homogeneously dispersed in the quaternary PNCs and the size is smaller than that in the ternary PNCs. Furthermore, OMMT in PPRS2 is mainly exfoliated and partly intercalated [Figure 2(e)], which does not agree

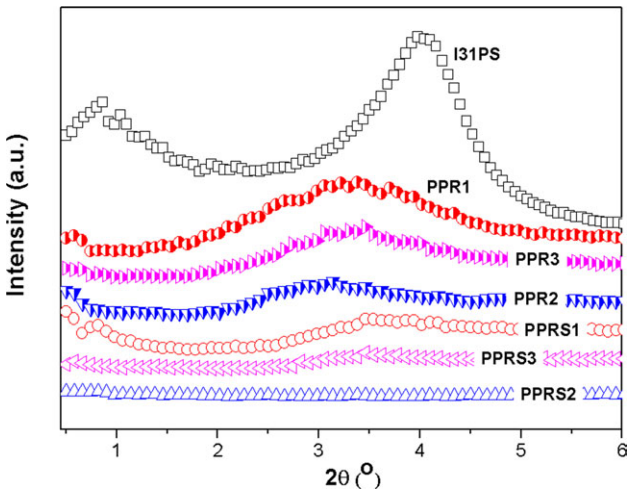

Figure 1. XRD patterns of the PNCs. [Color figure can be viewed in the online issue, which is available at wileyonlinelibrary.com.]

Applied Polymer SCIENCE

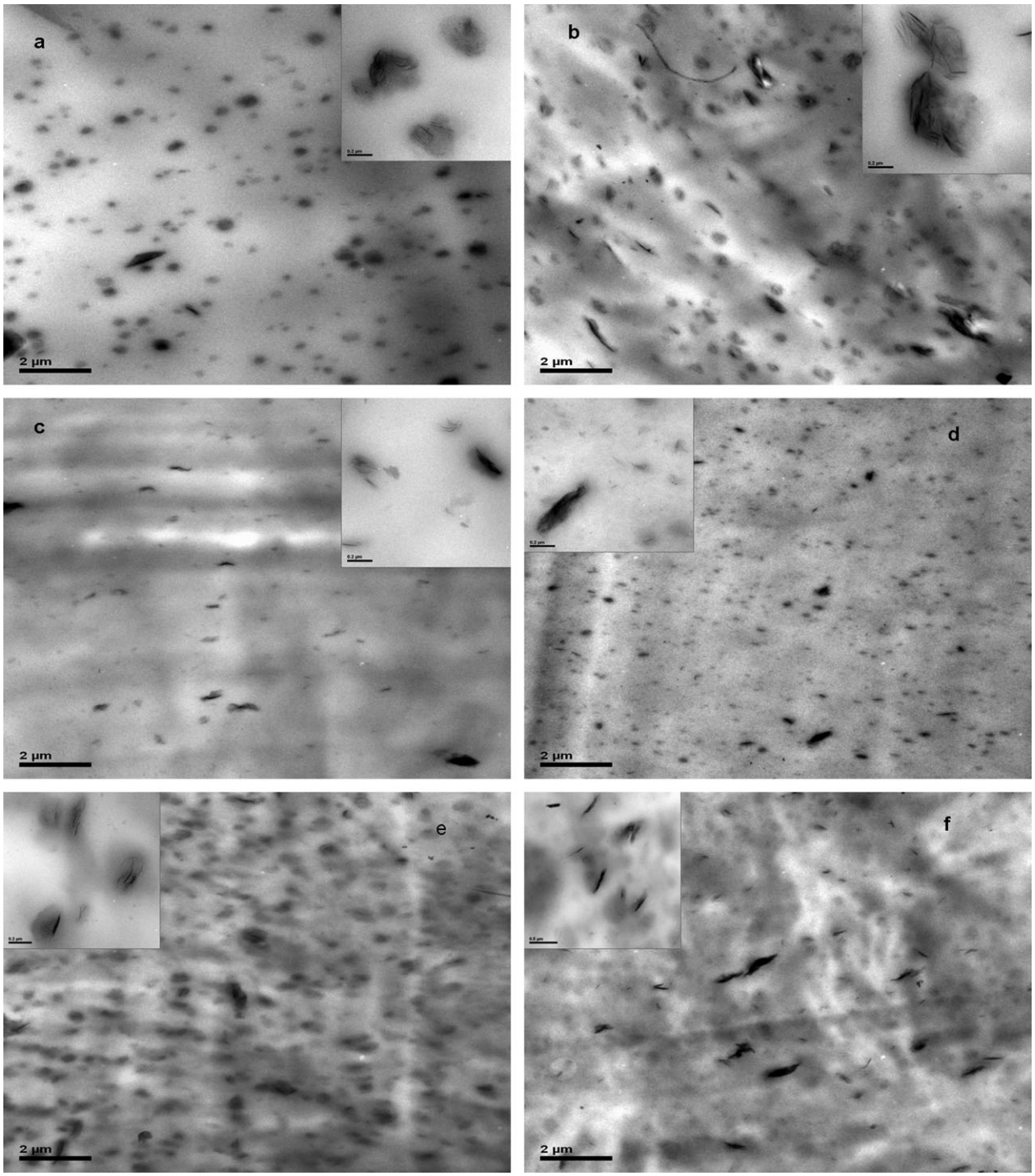

Figure 2. TEM images of PPR1 (a), PPR2 (b), PPR3 (c), PPRS1 (d), PPRS2 (e), PPRS3 (f).

with the XRD result. In fact, even for the zoomed-out small TEM image [inset in Figure 2(e)], the intercalation effect is still evident with small number of OMMT stacked layers. The exfoliation might be localized with the dominant intercalated structures. The disappearance of XRD peak of PPRS2 in Figure 1 might result from the randomly distributed structures of OMMTs, which could not be easily detected in periodic structural analysis in XRD. Besides, the location of OMMT is sensitive to compatibilizer and SEBS. For the PNCs containing PPB-*g*-MA, OMMT in PPR3 is totally located in the PPR phase while that in PPRS3 is mainly located in SEBS phase and partially in PPR phase. For the PNCs containing SEBS-*g*-MA or POE-*g*-MA, OMMT in PPR1 and PPR2 is surrounded by the compatibilizers while OMMT in PPRS1 and PPRS2 is located in the SEBS phase with enrichment in the PPR-SEBS interface. These results indicate that the rigid OMMT aggregates would

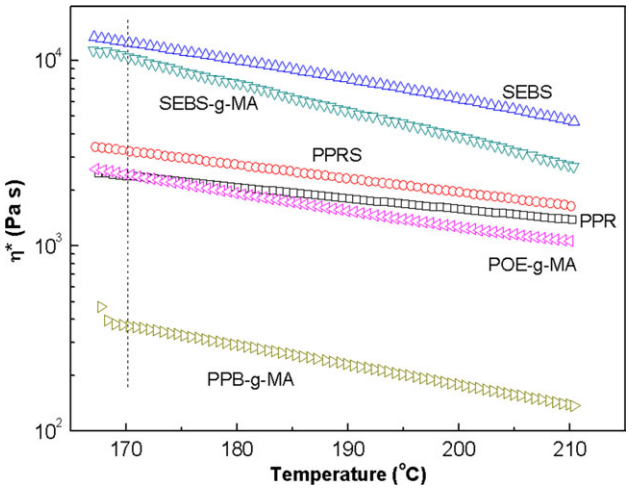

Figure 3. Complex viscosity η^* of matrixes and compatibilizers against temperature. [Color figure can be viewed in the online issue, which is available at wileyonlinelibrary.com.]

be covered by elastomer SEBS or elastomeric compatibilizers SEBS-*g*-MA and POE-*g*-MA to form a soft core-shell encapsulation structure. The core-shell phase morphology with organoclay layers encapsulated by elastomer has been observed in ternary PP/elastomer/filler composites.[15,25–30]

Figure 3 shows complex viscosity η^* against temperature for PPR, SEBS, the PPR/SEBS (85/15 by weight) blend (PPRS) and the three different compatibilizers. As seen in Figure 3, SEBS exhibits higher η^* and smaller temperature dependence than PPR so that blending SEBS with PPR leads to the blend matrix (PPRS) with slightly increased η^* and reduced temperature dependence in comparison with the PPR matrix. Because of the higher η^* of SEBS than PPR, SEBS can bear higher shearing stress during melting compounding,[24,31,32] which facilitates the OMMT uniform dispersion and improves the exfoliation dispersion degree, resulting in the OMMT preferential distribution in SEBS domains.[33,34]

Among the three compatibilizers, SEBS-*g*-MA exhibits η^* considerably higher than PPR and PPRS and the reverse is true for PPB-*g*-MA. On the other hand, η^* of POE-*g*-MA is close to those of PPR and PPRS. Though molecular structure of compatibilizer and its compatibility with the matrix might influence the OMMT dispersion, the viscosity matching may be one of the dominative factors. SEBS-*g*-MA has a better affinity to SEBS than to PPR. At the processing temperature, SEBS-*g*-MA with η^* much higher than PPR tends to encapsulate OMMT in PPR1 while it promotes OMMT to preferentially distribute in the SEBS domains in PPRS1, which leads to more OMMT exfoliation dispersion and smaller OMMT sizes in PPRS1 [inset in Figure 2(b)] than in PPR1 [inset in Figure 2(a)]. Though POE-*g*-MA is highly incompatible with PPR,[24] the two polymers have almost the same M_w and M_w/M_n (Table I) as well as η^* in the processing temperature range, allowing small POE-*g*-MA domains with encapsulated OMMT mixing with PPR rather homogeneously and facilitating PPR intercalation into OMMT. η^* of POE-*g*-MA is much lower than SEBS, but it in combination with SEBS exhibits the strongest effect to exfoliate OMMT in PPRS2 possibly due to the preferential distribution of OMMT in the SEBS domains and the good affinity between POE-*g*-MA and SEBS. PPB-*g*-MA exhibits the weakest compatibilization effect, making OMMT partial aggregation in both the ternary (PPR3) and the quaternary PNCs (PPRS3), which might be attributed to its melt viscosity considerably lower than those of PPR and PPRS. During melt compounding, PPB-*g*-MA probably forms liquid-drops dispersed in the matrixes, which directly hinders the compatibilization effect for polymer intercalation into OMMT. Introduction of SEBS in PPRS3 could improve OMMT dispersion to some extent while OMMT tactoids still exist, which is attributed to the high affinity of PPB-*g*-MA to PPR rather than SEBS so that quite a few stacked OMMT encapsulated by SEBS could not be effectively sheared and intercalated during melt blending. In a word, the dispersion and the distribution of OMMT in PNCs highly depend on chemical structure of compatibilizer, viscosity matching, and molecular interaction between the compatibilizer and the matrix at the blending temperature.[24,26,31,32]

Rheological Behaviors of PNCs

Rheology is very sensitive to the filler dispersion in composites. Molten PNCs usually exhibit a solid-like behavior at low frequencies under small-amplitude oscillatory shear flow, which has been used to detect the extent of delamination and dispersion of silicates.[5,22,35,36]

Figure 4 shows ω-sweep of PPR and PPRS as well as the ternary and the quaternary PNCs at 180°C. The quaternary PNCs demonstrate higher storage modulus (G') [Figure 4(a)], η^* [Figure 4(b)] and lower tanδ values [Figure 4(c)] in the low-ω region than the ternary PNCs. Additions of both SEBS and OMMT improve the elastic behavior[22] due to the partial compatibility between SEBS and PPR as well the hydrodynamic reinforcement effect of OMMT, respectively. In the ternary PNCs, compatibilizer PPB-*g*-MA leads to the highest degree of aggregation of intercalated OMMT, which is responsible for the lowest G'. On the other hand, in the quaternary PNCs, SEBS-*g*-MA is more helpful for dispersion of intercalated OMMT other than PPB-*g*-MA, resulting in the higher G'. The more exfoliated PPRS2 with compatibilizer POE-*g*-MA exhibits the highest G' and η^* among the quaternary PNCs, which could be ascribed to the long time relaxation of percolated network of exfoliated silicate platelets. Nevertheless, the enhanced G' and η^* and the reduced tanδ are mainly caused by the addition of SEBS while the effect of OMMT dispersion on the rheological variation is unobvious. This seems to be consistent with the XRD pattern that scarcely changes by various compatibilizers except for PPRS2.

Solid-like behavior in PNCs melt is usually related to the formation of a transient network by molecular entanglement and chain adsorption on filler surface or a percolated filler network,[37,38] which is reflected from the reduced low-ω slope of G' and the appearance of a tanδ peak. Meanwhile, "tail-up" phenomenon of Cole–Cole curve is usually used to characterize the pseudo-solid behavior in PNCs melts. Figure 4(d) shows Cole–Cole plots of loss viscosity (η'') as a function of storage viscosity (η'). According to the Cole–Cole plots, the rest time of the quaternary PNCs is all longer than the ternary ones.

Applied Polymer SCIENCE

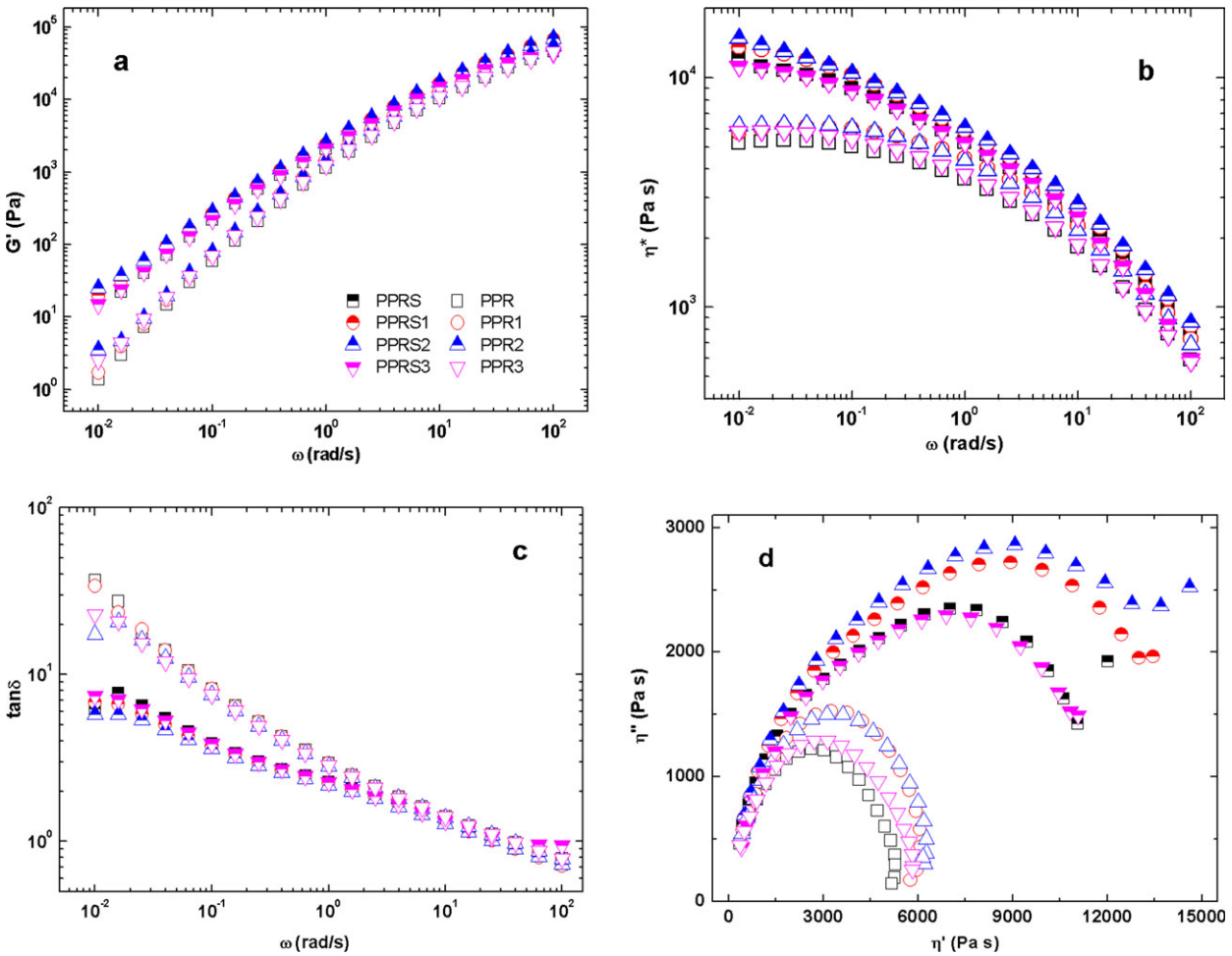

Figure 4. Storage modulus G' (a), complex viscosity η^* (b) and Tanδ (c) as function of frequency ω and Cole–Cole plot of loss viscosity η'' against dynamic viscosity η' (d) for the PNCs at 180°C. [Color figure can be viewed in the online issue, which is available at wileyonlinelibrary.com.]

Moreover, the curves of PPRS, PPRS1, and PPRS2 exhibit "tail-up" phenomenon at $\omega < 0.026$ rad/s, indicating a phase separated structure in PPRS and a percolated filler network in PPRS1 and PPRS2. The "tail-up" phenomenon is not observed in the quaternary PNCs containing low-viscosity PPB-*g*-MA and all the ternary PNCs.

Figure 5(a) shows steady viscosity (η) as function of shear rate ($\dot{\gamma}$) and Table II lists critical shear rate for thinning $\dot{\gamma}_c$, and zero-shear viscosity η_0 for the PNCs at 180°C. The PNCs exhibit Newtonian plateaus in the low-$\dot{\gamma}$ region followed with a significant shear-thinning in the high-$\dot{\gamma}$ region.[39–42] In comparison with the ternary PNCs, the quaternary ones demonstrate elevated flow curves, which is in agreement with dynamic rheology in Figure 4(b). η_0 of quaternary PNCs increases with the increase of the intercalation and exfoliation dispersion degrees (Figures 1 and 2 and Table II). Meanwhile, $\dot{\gamma}_c$ of quaternary PNCs is lower than the ternary ones, indicating that the presence of SEBS promotes the molecular disentanglement under shear action.

A time-concentration superposition (TCS) is proved to be a useful tool to analyze the microstructure of filled polymer melts using a $\dot{\gamma}$ shift factor $a_{\dot{\gamma}}$ and a viscosity shift factor $1/a_n$ for steady rheology.[39] Shift factors a_n and $a_{\dot{\gamma}}$ reflect the reinforcement effect caused by addition of rigid OMMT and the strain amplification effect caused by the enhanced shear deformation of polymer fluid between rigid OMMT inclusions, respectively. Shifting the steady flow data of PNCs along the viscosity and the shear rate axes allows establishing respective master curves with PPR and PPRS as references, as shown in Figure 5(b). The data superposition suggests that the presence of OMMT aggregates does not influence the mechanism for onset of nonlinear steady flow involved in the molecular disentanglement of the matrix without breakdown of OMMT tactoids and desorption of polymer chains absorbed on OMMT surface. Eslami et al.[39] found a strong shear-thinning and a significant increase in η at low shear rates when clay loadings are above the percolation threshold. The shear-thinning in η at low shear rates is not observed in the PNCs here because of the low OMMT content. Inset in Figure 5(b) shows shift factors a_n and $a_{\dot{\gamma}}$ of the PNCs. It is seen that both a_n and $a_{\dot{\gamma}}$ are in the range of 1.0–1.1 in the ternary PNCs, revealing that the reinforcement and the strain amplification effects are neglectable considering the low OMMT

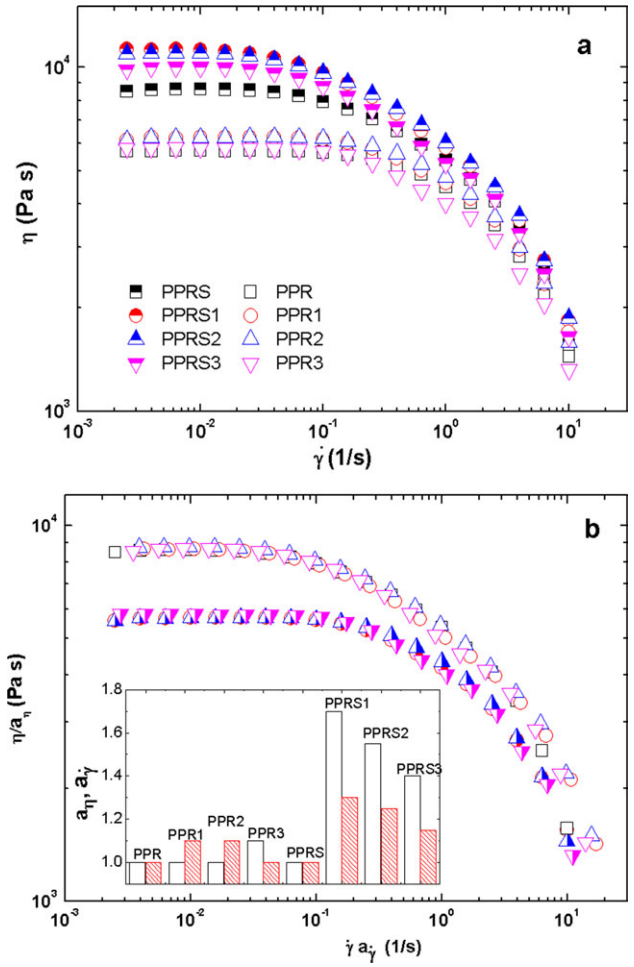

Figure 5. Steady viscosity η against shear rate $\dot{\gamma}$ (a) and master curves of η/a_η against $a_{\dot{\gamma}}\dot{\gamma}$ (b) for the PNCs at 180°C. The inset in (b) shows shift factors a_η (shadowed) and $a_{\dot{\gamma}}$ (white). [Color figure can be viewed in the online issue, which is available at wileyonlinelibrary.com.]

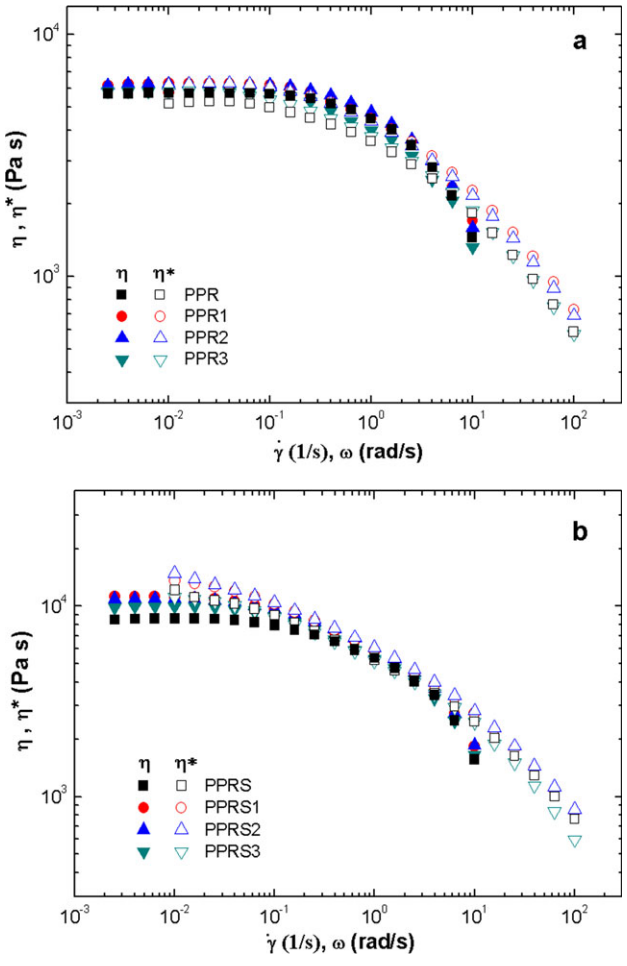

Figure 6. Steady viscosity $\eta(\dot{\gamma})$ against shear rate $\dot{\gamma}$ and complex viscosity $\eta^*(\omega)$ against frequency ω for the PPR series PNCs (a) and the PPRS series PNCs (b) at 180°C. [Color figure can be viewed in the online issue, which is available at wileyonlinelibrary.com.]

content. On the other hand, the two effects become significant in the quaternary PNCs, revealing the importance of SEBS in adjusting the OMMT dispersion. It is the fine dispersion of OMMT aggregates with small size in the quaternary PNCs causes the lager a_n and $a_{\dot{\gamma}}$ values than the ternary PNCs.

Empirical Cox–Merz rule $\eta*(\omega) = \eta(\dot{\gamma})|_{\omega=\dot{\gamma}}$ has been found to be valid for rheology-simple polymer systems while it usually fails for PNCs and many mesostructured materials.[39,42,43] Figure 6 compares $\eta^*(\omega)$ and $\eta(\dot{\gamma})$ for the PNCs. Cox–Merz rule in general holds for monophasic PPR and the ternary PNCs

Table III. Tensile and Izod Impact Properties of the PNCs

				Izod impact strength (kJ/m^2)	
Sample code	Yield stress (MPa)	Strain at break (%)	Tensile modulus (MPa)	30°C	−23°C
PPR	28 ± 0.3	1262 ± 29	367 ± 12	3.9 ± 0.1	3.5 ± 0.2
PPR1	28 ± 0.1	305 ± 26	327 ± 8	3.0 ± 0.2	2.1 ± 0.3
PPR2	28 ± 0.2	224 ± 33	338 ± 16	4.9 ± 0.4	3.4 ± 0.2
PPR3	30 ± 0.2	211 ± 55	358 ± 27	2.6 ± 0.2	2.7 ± 0.1
PPRS	18 ± 0.5	1021 ± 28	170 ± 6	23.9 ± 3.1	12.4 ± 0.9
PPRS1	17 ± 0.2	476 ± 119	169 ± 6	19.4 ± 1.4	8.9 ± 0.8
PPRS2	19 ± 0.5	1022 ± 28	166 ± 8	40.5 ± 3.5	12.6 ± 1.7
PPRS3	21 ± 0.2	916 ± 38	187 ± 6	8.4 ± 0.4	6.7 ± 0.5

Applied Polymer SCIENCE

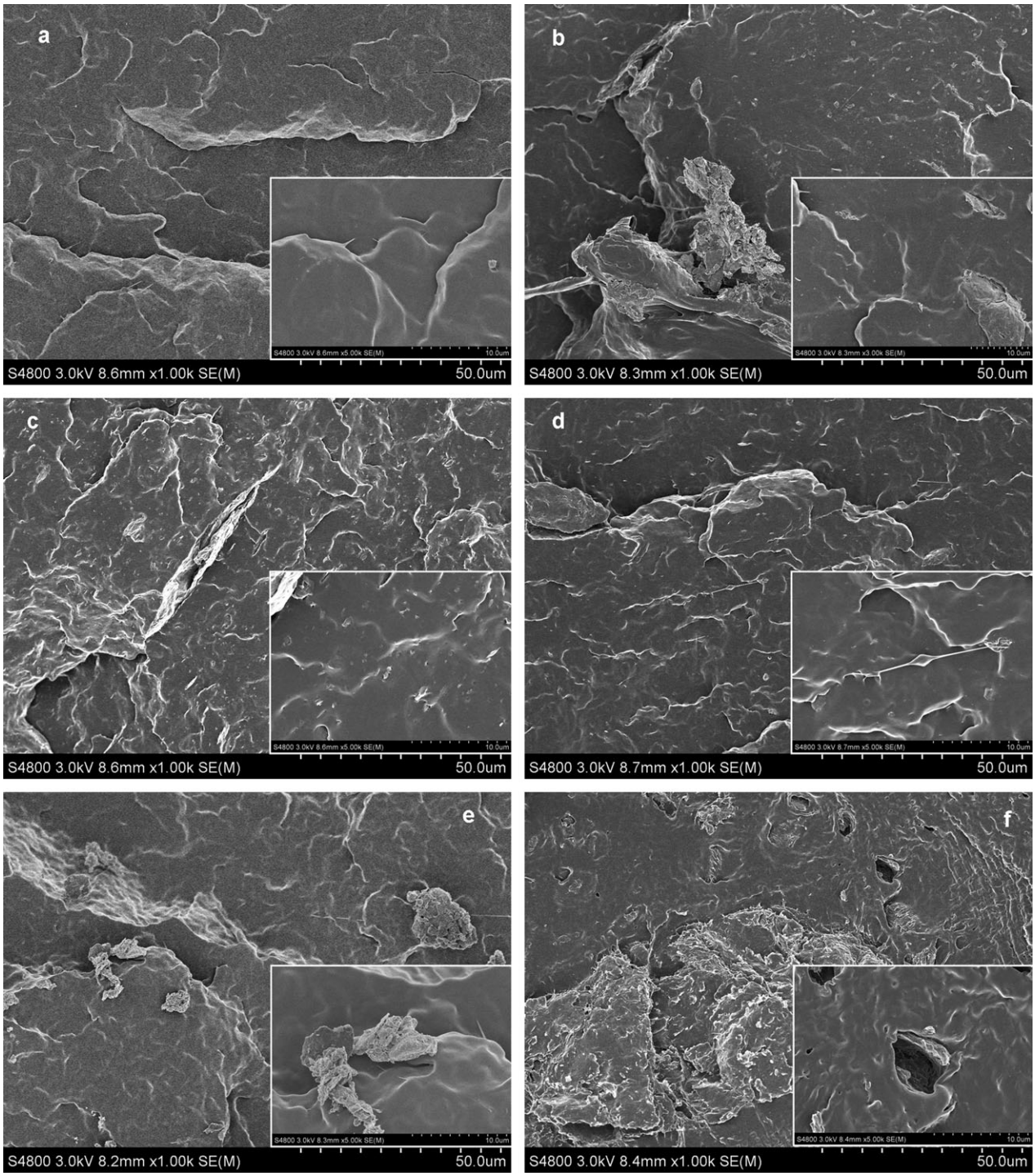

Figure 7. SEM micrographs showing impact fracture surfaces of PPR (a), PPR1 (b), PPR2 (c), PPR3 (d), PPRS (e), PPRS1 (f), PPRS2 (g), PPRS3 (h).

because of the low contents of OMMT (2 phr) and compatibilizer (3 phr). However, this rule fails in biphasic PPRS and the quaternary PNCs at the low-ω ($\dot{\gamma}$) side. Ren and Krishnamoorti[43] found that $\eta^*(\omega)$ may exceed $\eta(\dot{\gamma})$ at low rates arising from change of mesoscale structure and orientation of highly anisotropic silicate layers or tactoids. In middle rate region, $\eta^*(\omega)$ and $\eta(\dot{\gamma})$ overlap with each other, indicating breakdown of network structure in the PPRS and PPRS series PNCs and some orientation of OMMT ("parallel" alignment) with increasing shear rate.[43]

Mechanical Properties of PNCs

Table III shows mechanical properties of PPR and PPRS as well as the PNCs. SEBS toughens PPR significantly,[16,19] resulting in

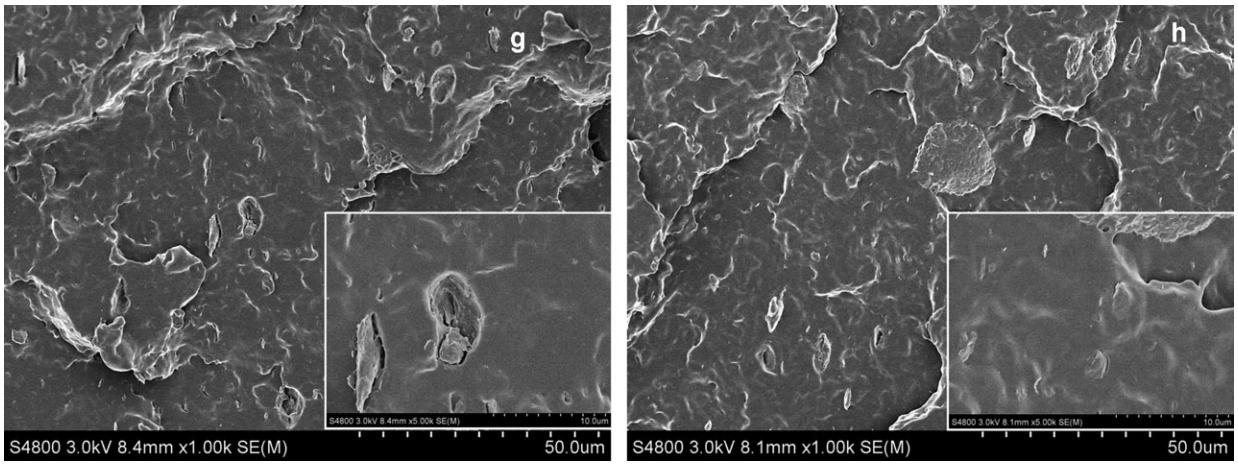

Figure 7. *(Continued)*

a marked increase in Izod impact strength accompanying with evident decreases in yield stress and tensile strength and a slight decrease in elongation at break. The above results imply a strong net interaction between SEBS and PPR. In comparison with the matrix, elongation at break of PNCs except for PPRS2 decreases evidently with addition of OMMT. The PNCs containing SEBS-*g*-MA and POE-*g*-MA exhibit reduced Young's modulus and the reverse is true for those containing PPB-*g*-MA. Using SEBS-*g*-MA and PPB-*g*-MA compatibilizers leads to reduction in impact strength in comparison with the matrix and the reverse is true for POE-*g*-MA compatibilizer. Thus PPR2 and PPRS2 exhibit the best comprehensive mechanical properties among the ternary and the quaternary PNCs, respectively. The results indicate that the mechanical properties of PNCs are directly related to the intercalation/exfoliation level of the clay dispersion and the interfacial bonding strength. The improved impact strength of PPR2 and PPRS2 in comparison with the matrix could be ascribed to POE-*g*-MA that facilitates the formation of more exfoliated OMMT located inside the elastomeric POE-*g*-MA domains[20,21] [Figure 2(b,e)]. On the other hand, the reduced impact strength for the PNCs containing SEBS-*g*-MA and PPB-*g*-MA may be related to the aggregated OMMT stacks in the matrix, which directly results in the decrease of interfacial interaction between the matrix and OMMT.

Figure 7 gives SEM micrographs of impact fracture surfaces of PNCs. All the PNCs show good distribution of OMMT particles. However, there are some delicate differences on the fracture surfaces of PNCs, which might be related to different impact toughness shown in Table III. The quaternary PNCs all display protrusions more than the ternary PNCs, indicating that the interfacial adhesive strength increased with addition of SEBS. Furthermore, there are some microvoids on the surface of PPRS1 [Figure 7(f)] attributed to voiding of elastomers due to strong interfacial adhesion. The elastomer voiding can consume mechanical energy during impact deformation but also facilitate the damage of PPRS1, resulting in a lower impact strength than PPRS. Moreover, some prominent cleavages can be found on the surface of PPRS2, which could be assigned to interfacial debonding between SEBS elastomeric domains and PPR matrix. The interfacial debonding contributes greatly to the improved impact strength of PPRS2 than PPRS especially at 30°C. It is the special distribution of OMMT in presence of POE-*g*-MA that promotes the interfacial adhesion probably involving in the OMMT-PPR interface, and this process also contributes to the improved toughness of PPR2 in comparison with PPR. For PPR1 and PPR3, there are no ways of energy consumption via voiding or interfacial debonding, resulting in lower toughness than PPR. The same is true for PPRS3 in comparison with PPRS.

Mechanical properties of the PNCs with the same OMMT content are highly dependent on compatibilizer. OMMT does not always improve rigidity but sometimes lowers Young's modulus, yielding stress, and toughness simultaneously upon addition SEBS-*g*-MA compatibilizer. This result is quite different from Bao and Tjong[18] who found that SEBS-*g*-MA can improve the compatibility of iPP and OMMT and thus enhances toughness of the PNCs. POE-*g*-MA as compatibilizer can improve toughness effectively without marked degradation in rigidity in comparison with the matrix. The dispersion and location of OMMT determine the mechanical properties. Additions of soft elastomers and rigid OMMT have been expected to form a percolated nanostructure for producing a synergistic effect for balancing toughness and stiffness.[17,20,22,44] However, it is the compatibilizer that plays a key role for the OMMT dispersion and the mechanical properties of the PNCs.

CONCLUSIONS

Compatibilizers significantly influence the structure and properties of the PNCs prepared via melt extrusion. SEBS could improve melt viscosity and impact toughness of the matrix and the PNCs while the compatibilizers influence the OMMT dispersion and the mechanical properties. Meanwhile, the mainly intercalated structure could be achieved in the PNCs except for the mainly exfoliated structure in the POE-*g*-MA compatibilized quaternary PNCs. POE-*g*-MA could facilitate OMMT to form a more exfoliated dispersion and thus toughen the PNCs without

marked degradation in rigidity. On the other hand, SEBS-*g*-MA leads to simultaneous reduction in strength, modulus, and toughness while PPB-*g*-MA is helpful for improving rigidity at the expense of toughness. The preferred balance between toughness and stiffness of the PPR and the PPRS series PNCs can be attained by the incorporations of POE-*g*-MA as compatibilizers and the presence of SEBS elastomeric component greatly improves impact toughness of PPRS2 in comparison with PPR2.

ACKNOWLEDGMENTS

The authors gratefully appreciate the financial supported from the Program for Zhejiang Provincial Innovative Research Team (No. 2009R50004).

REFERENCES

1. Kumar, A. P.; Depan, D.; Tomer, N. S.; Singh, R. P. *Prog. Polym. Sci.* **2009**, *34*, 479.
2. Krump, H.; Thompson, M. R. *Kgk-Kaut. Gummi. Kunst.* **2010**, *63*, 493.
3. Ghasemi, H.; Carreau, P. J.; Kamal, M. R.; Chapleau, N. *Int. Polym. Proc.* **2011**, *26*, 219.
4. Manikantan, M. R.; Varadharaju, N. *Packag. Technol. Sci.* **2011**, *24*, 191.
5. Elleithy, R.; Chafidz, A.; Ali, M. A. H. *J. Mater. Sci.* **2011**, *46*, 6075.
6. Tjong, S. C.; Bao, S. P.; Hang, G. D. *J. Polym. Sci. Polym. Phys.* **2005**, *43*, 3112.
7. Liu, S. P.; Liang, C. W. *Int. Commun. Heat Mass* **2011**, *38*, 434.
8. Paul, D. R.; Kim, D. H.; Fasulo, P. D.; Rodgers, W. R. *Polymer* **2007**, *48*, 5308.
9. Chrissopoulou, K.; Altintzi, I.; Andrianaki, I.; Shemesh, R.; Retsos, H.; Giannelis, E. P.; Anastasiadis, S. H. *J. Polym. Sci. Polym. Phys.* **2008**, *46*, 2683.
10. Osman, M. A.; Mittal, V.; Suter, U. W. *Macromol. Chem. Phys.* **2007**, *208*, 68.
11. Dong, Y.; Bhattacharyya, D. *Mater. Sci. Eng. A-Struct.* **2010**, *527*, 1617.
12. Liu, S. P. *Polym. Compos.* **2011**, *32*, 1389.
13. Sun, T. C.; Dong, X.; Du, K.; Wang, K.; Fu, Q.; Han, C. C. *Polymer* **2008**, *49*, 588.
14. Chow, W. S.; Abu Bakar, A.; Ishak, Z. A. M.; Karger-Kocsis, J.; Ishiaku, U. S. *Eur. Polym. J.* **2005**, *41*, 687.
15. Sun, T. C.; Chen, F. H.; Dong, X.; Han, C. C. *Polymer* **2008**, *49*, 2717.
16. Setz, S.; Stricker, F.; Kressler, J.; Duschek, T.; Mulhaupt, R. *J. Appl. Polym. Sci.* **1996**, *59*, 1117.
17. Kusmono, Z. A.; Ishak, M.; Chow, W. S.; Takeichi, T.; Rochmadi. *Eur. Polym. J.* **2008**, *44*, 1023.
18. Bao, S. P.; Tjong, S. C. *Compos. Part A Appl. Sci.* **2007**, *38*, 378.
19. Nishitani, Y.; Ohashi, K.; Sekiguchi, I.; Ishii, C.; Kitano, T. *Polym. Compos.* **2010**, *31*, 68.
20. Martin, Z.; Jimenez, I.; Gomez, M. A.; Ade, H.; Kilcoyne, D. A. *Macromolecules* **2010**, *43*, 448.
21. Martin, Z.; Jimenez, I.; Gomez-Fatou, M. A.; West, M.; Hitchcock, A. P. *Macromolecules* **2011**, *44*, 2179.
22. Su, F. H.; Huang, H. X. *J. Appl. Polym. Sci.* **2009**, *112*, 3016.
23. Ishak, M.; Kusmono, Z. A.; Chow, W. S.; Takeichi, T.; Rochmadi. *Compos. Part A Appl. Sci.* **2008**, *39*, 1802.
24. Lai, S. M.; Chen, W. C.; Zhu, X. S. *Compos. Part A Appl. Sci.* **2009**, *40*, 754.
25. Lim, J. W.; Hassan, A.; Rahmat, A. R.; Wahit, M. U. *Polym. Plast. Technol.* **2008**, *47*, 411.
26. Kim, K. N.; Kim, H.; Lee, J. W. *Polym. Eng. Sci.* **2001**, *41*, 1963.
27. Premphet, K.; Horanont, P. *J. Appl. Polym. Sci.* **2000**, *76*, 1929.
28. Pukanszky, B.; Tudos, F.; Kolarik, J.; Lednicky, F. *Polym. Compos.* **1990**, *11*, 98.
29. Kolarik, J.; Lednicky, F.; Jancar, J.; Pukanszky, B. *Polym. Commun.* **1990**, *31*, 201.
30. Fortelny, I.; Kamenicka, D.; Kovar, J. *Angew. Makromol. Chem.* **1988**, *164*, 125.
31. Kawasumi, M.; Hasegawa, N.; Kato, M.; Usuki, A.; Okada, A. *Macromolecules.* **1997**, *30*, 6333.
32. Wang, Y.; Chen, F. B.; Wu, K. C.; Wang, J. C. *Polym. Eng. Sci.* **2006**, *46*, 289.
33. Zhu, Y.; Ma, H. Y.; Tong, L. F.; Fang, Z. P. *Chin. J. Polym. Sci.* **2008**, *26*, 783.
34. Fang, Z. P.; Zhu, Y.; Chen, Y. *J. Acta Polym. Sin.* **2009**, 145.
35. Qiao, X. Y.; Zhong, W. X.; Sun, K.; Chen, X. D. *J. Appl. Polym. Sci.* **2009**, *114*, 1702.
36. Abdel-Goad, M. *Compos Part B Eng* **2011**, *42*, 1044.
37. Zhang, X. W.; Pan, Y.; Zheng, Q.; Yi, X. S. *J. Appl. Polym. Sci.* **2002**, *86*, 3173.
38. Mungall, J. E. *Phys. Rev. Lett.* **1994**, *73*, 288.
39. Eslami, H.; Grmela, M.; Bousmina, M. *J. Rheol.* **2010**, *54*, 539.
40. Cassagnau, P. *Polymer* **2008**, *49*, 2183.
41. Vermant, J.; Ceccia, S.; Dolgovskij, M. K.; Maffettone, P. L.; Macosko, C. W. *J. Rheol.* **2007**, *51*, 429.
42. Krishnamoorti, R.; Banik, I.; Xu, L. *Rev. Chem. Eng.* **2010**, *26*, 3.
43. Ren, J. X.; Krishnamoorti, R. *Macromolecules* **2003**, *36*, 4443.
44. Ohlsson, B.; Hassander, H.; Tornell, B. *Polymer* **1998**, *39*, 6705.